This document is confidential and is proprietary to the American Chemical Society and its authors. Do not copy or disclose without written permission. If you have received this item in error, notify the sender and delete all copies.

Influence of $LaFeO_3$ Surface Termination on Water Reactivity

Journal:	*The Journal of Physical Chemistry Letters*
Manuscript ID	jz-2017-00195w.R1
Manuscript Type:	Letter
Date Submitted by the Author:	n/a

Complete List of Authors:	Stoerzinger, Kelsey; Pacific Northwest National Laboratory, Physical and Computational Sciences Directorate Comes, Ryan; Pacific Northwest National Laboratory, Physical and Computational Sciences Directorate; Auburn University, Physics Spurgeon, Steven; Pacific Northwest National Lab, Physical and Computational Sciences Directorate Thevuthasan, Suntharampillai; Pacific Northwest National Laboratory, Physical and Computational Sciences Directorate Ihm, Kyuwook; Pohang Accelerator Laboratory Crumlin, Ethan; E O Lawrence Berkeley National Laboratory, Advanced Light Source Chambers, Scott; Pacific Northwest National Laboratory, Physical and Computational Sciences Directorate

SCHOLARONE™
Manuscripts

Influence of $LaFeO_3$ Surface Termination on Water Reactivity

Kelsey A. Stoerzinger,[1,] Ryan Comes,[1,2] Steven R. Spurgeon,[1] Suntharampillai Thevuthasan,[1] Kyuwook Ihm,[3] Ethan J. Crumlin,[4] Scott A. Chambers,[1,*]*

[1]Physical and Computational Sciences Directorate, Pacific Northwest National Laboratory, Richland, Washington 99352, USA

[2]Department of Physics, Auburn University, Auburn, Alabama 36849, USA

[3]Pohang Accelerator Laboratory, Pohang, Kyungbuk, Korea

[4]Advanced Light Source, Lawrence Berkeley National Laboratory, Berkeley, California 94720, USA

AUTHOR INFORMATION

Corresponding Author

*kelsey.stoerzinger@pnnl.gov; sa.chambers@pnnl.gov

ABSTRACT The polarity of oxide surfaces can dramatically impact their surface reactivity, in particular with polar molecules such as water. The surface species that result from this interaction change the oxide electronic structure and chemical reactivity in applications such as

photoelectrochemistry, but are challenging to probe experimentally. Here we report a detailed study of the surface chemistry and electronic structure of the perovskite $LaFeO_3$ in humid conditions using ambient pressure X-ray photoelectron spectroscopy. Comparing the two possible terminations of the polar (001)-oriented surface, we find that the LaO-terminated surface is more reactive toward water, forming hydroxyl species and adsorbing molecular water at lower relative humidity than its FeO_2-terminated counterpart. However, the FeO_2-terminated surface forms more hydroxyl species during water adsorption at higher humidity, suggesting adsorbate-adsorbate interactions may impact reactivity. Our results demonstrate how the termination of a complex oxide can dramatically impact its reactivity, providing insight that can aid in the design of catalyst materials.

TOC GRAPHICS

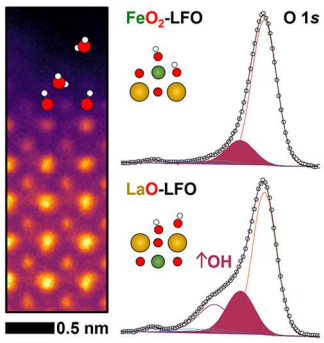

Perovskite oxides such as $LaFeO_3$ show great promise as catalysts for energy conversion and storage. Applications such as electrocatalysis,[1–4] photoelectrochemistry,[5–7] and gas sensing[8–10] all take place in an aqueous or humid environment, where the interaction with water plays a key role in determining the functionality of these complex oxides.[11–13] The formation of surface hydroxyl groups and adsorption of water can impact the surface electronic structure[14] and ultimately the mechanisms and kinetics of surface chemical reactions.[15,16] Initial studies have considered the reactivity of perovskites with water using ambient pressure X-ray photoelectron spectroscopy

(AP-XPS),[12,17] enabling study of the surface species present in equilibrium with water vapor. The hydroxylation of these surfaces appeared greater than that of binary transition metal oxides.[18] However, the chemical nature of the hydroxyl site in such systems remained elusive due to the unknown surface termination.

The polar layers of (001)-oriented polar perovskite $LaFeO_3$ (LFO) have been the subject of numerous recent investigations that consider the dipole formed at the (Nb-doped) $SrTiO_3$ substrate-film interface[19–21] and the formation of a 2D metal at this interface[22]. However, despite the promising photoelectrochemical activity[5] and sensing capabilities,[9,10] missing is an experimental understanding of the surface properties for each layer. Density functional theory (DFT) calculations report a lower work function for LaO- versus FeO_2-termination,[23] which is expected to result in notably different chemical reactivity. Of further interest is how the electronic structure of each surface changes as a result of the formation of e.g. hydroxyl species, where surface band bending in aqueous environments[24] is the critical component to charge separation at the semiconductor/water interface in photoelectrochemical water splitting.

In the present work, we consider (001)-oriented epitaxial films of LFO distinctly terminated on $(LaO)^+$ or $(FeO_2)^-$ planes to probe the influence of perovskite surface termination on chemical reactivity using ambient pressure X-ray photoelectron spectroscopy (AP-XPS).[18,25,26] We find LaO-terminated LFO (LaO-LFO) is more reactive toward water, forming hydroxyl species at lower relative humidities than its FeO_2-terminated (FeO_2-LFO) counterpart, consistent with DFT calculations that indicate a greater stability of hydroxylated LaO-LFO.[12] The LaO surface is also characterized by an additional surface oxygen species in both dry and humid conditions, the formation of which is attributed to the positive charge of a $(LaO)^+$ layer and its high surface energy. Core level shifts and changes in the gas-phase water peak indicate a downward band

bending/flattening[27] and a decrease in work function,[28] respectively, resulting from hydroxylation and water adsorption.

Epitaxial 9 unit cell (u.c.) LFO films were fabricated by oxygen-assisted molecular beam epitaxy (MBE) on Nb-doped $SrTiO_3$ (001) surfaces at Pacific Northwest National Laboratory (Figure S1). The substrate was prepared with SrO or TiO_2 termination, resulting in LaO-LFO or FeO_2-LFO, respectively (Figure 1). Cross-sectional high-angle annular dark field (STEM-HAADF) images, shown in Figure 1, confirm the excellent quality and epitaxy of the film. We observe differences in the surface termination, although damage resulting from TEM sample preparation makes it difficult to unambiguously identify the surface layer. Instead, the termination of the as-prepared film was confirmed by angle resolved XPS (Table S1) and remained unchanged during AP-XPS experiments (Figure S2).

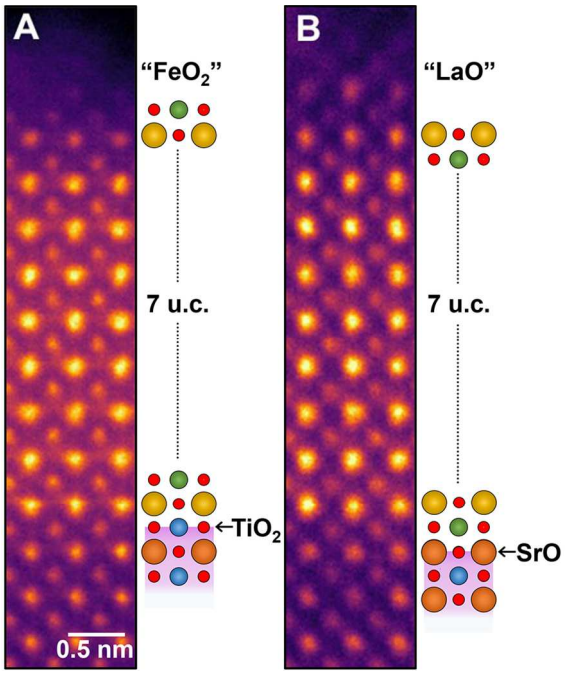

Figure 1. Colorized cross-sectional STEM-HAADF images and schematics of the 9 unit cell (u.c.) $LaFeO_3$/Nb:$SrTiO_3$ films fabricated by oxygen assisted MBE. FeO_2-LFO was grown on a

TiO_2-terminated substrate (A), and LaO-LFO was grown on a SrO-terminated one (B). Surface terminations were confirmed by angle resolved XPS (Table S1).[19]

Upon introduction to the AP-XPS chamber at the Advanced Light Source, the films were cleaned of ambient carbon contaminants by heating to 300 °C in 100 mTorr oxygen. The resulting O 1s spectra are compared in Figure 2 (top panel) for the LaO- and FeO_2-terminated surface, with the C 1s spectra shown in the inset. For the FeO_2-LFO, one main O 1s peak is present, characteristic of bulk lattice oxygen, with a small shoulder at ~1.1 eV higher binding energy attributed to hydroxyl (OH) species, the location of which was determined from difference spectra during subsequent water dosing (Figure S3). For LaO-LFO, a third peak is present at ~2.3 eV higher binding energy, termed "surf". Such a surface feature has been often observed for epitaxial perovskite films of unknown termination, as well as perovskite particles, and has been attributed to a host of potential species such as carbonates,[29,30] adsorbed water,[31,32] hydroxyls,[31–33] peroxide species,[34] undercoordinated oxygen,[35,36] and the terminal layer(s) of a polar surface due to a shift in Madelung potential.[17] Considering the AP-XPS spectra collected at 300 °C in 100 mTorr oxygen (and similarly at ~24 mTorr oxygen, Figure S4), we rule out the presence of carbonates and adsorbed water, and the lack of such a feature on the FeO_2-terminated surface suggests it does not arise from a change in Madelung potential at the surface. Instead, we propose that the feature at ~2.3 eV above bulk oxygen arises from oxygen species present on the surface with reduced screening, where DFT calculations on MgO surfaces support such a binding energy offset for peroxo groups,[34] although a similar offset is also reported for OH groups on MgO.[37] The higher surface energy of the LaO- versus FeO_2-terminated surface predicted by DFT[12] supports the model that the $(LaO)^+$ surface reconstructs chemically (adsorbing additional oxygen) and/or electronically to compensate its polarity, while the $(FeO_2)^-$ surface seems stable

with only formation of a few hydroxyl groups (Figure 2B). A similar feature is observed on the SrO-terminated surface of (001)-oriented $SrTiO_3$, but not for the TiO_2 termination (Figure S5).

We next perform a water isobar to probe the LFO surfaces under different relative humidity (RH). After removing oxygen gas, 100 mTorr H_2O is introduced into the chamber at 300 °C (corresponding to a RH of 10^{-4}%). The OH feature on LaO-LFO increases notably, while that on FeO_2-LFO increases only slightly (Figure 2 middle panel). The feature at ~2.3 eV on LaO-LFO from undercoordinated oxygen/peroxo species persists in humid environments, which might protonate with minimal shift in binding energy. A peak from gas phase water is present at >5 eV higher binding energy than bulk oxygen. Further cooling leads to the formation of adsorbed water (H_2O_{ads}) at ~3.4 eV above bulk oxygen (Figure 2 bottom panel), the location of which is confirmed by difference spectra upon removal of water (Figure S6). The wider bulk peak at higher temperatures is consistent with thermal (vibrational) broadening. Due to the high propensity of LFO to form carbonate upon interaction with any residual CO_2 in the chamber,[38] care was taken to quantify such species in the O 1s spectra from the intensity in the C 1s core level (Experimental methods). All spectra were fit with the species described above with fitting parameters found in Table S2, and depth profiling by changing the incident photon energy confirms that the "surf" peak, OH, CO_3, and H_2O_{ads} are located above that of the bulk (Figure S7).

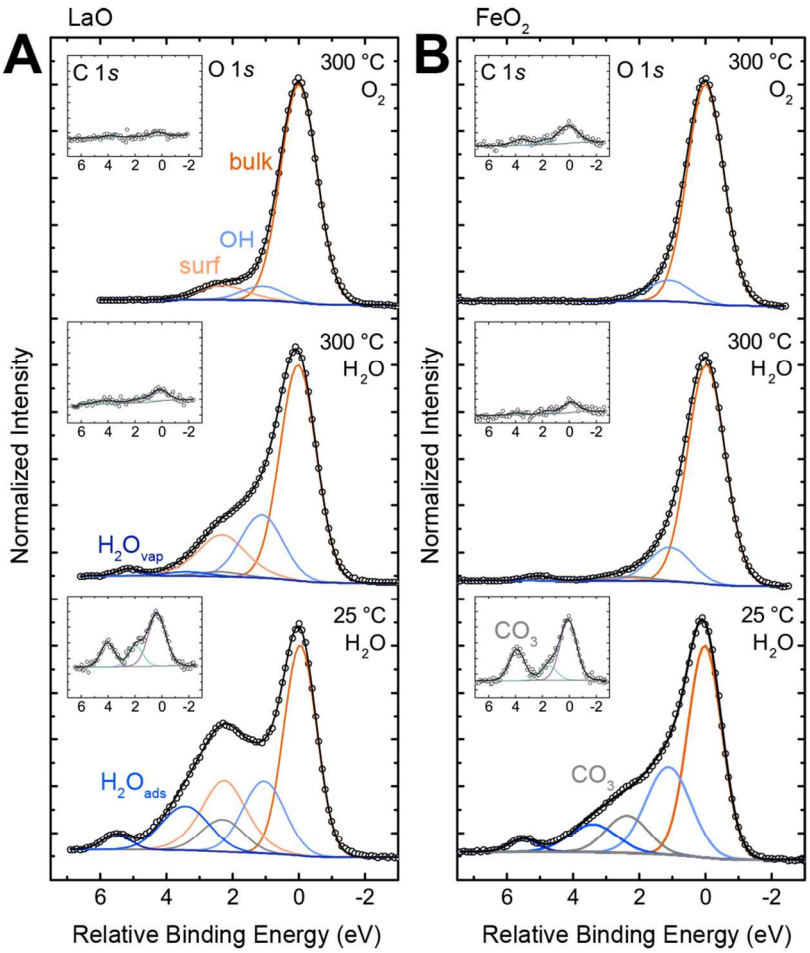

Figure 2. O 1s spectra and C 1s spectra (inset) for (A) LaO-LFO and (B) FeO_2-LFO at 300 °C in 100 mTorr O_2 (top), 300 °C in 100 mTorr H_2O (middle) and 25 °C in 100 mTorr H_2O (bottom). Raw data are shown as points with fitted components and envelope (black) as lines. O 1s components correspond to the bulk oxide (orange), hydroxide (light blue), carbonate (gray), surface (peach), adsorbed water (medium blue), and gas phase water (dark blue). C 1s components correspond to carbonate (gray), adventitious carbon (purple), and an intermediate carbon oxidation (teal). The binding energy scale is shown relative to the bulk oxide (O 1s) and adventitious carbon (C 1s) to better illustrate relative offsets of species in fitting.

The chemical reactivity of each surface toward water can be assessed by considering the extent of hydroxyl species present as a function of RH. Figure 3A compares the OH and H_2O_{ads} components normalized to the bulk oxygen signal (likely canceling out any thermal broadening effects), with similar trends observed when considering them as a percentage of total oxygen signal (Figure S8) or using a multilayer electron attenuation model[17] to compute coverage (Figure S9, Table S3). Both terminations display similar OH contents in dry conditions (300 °C in 100 mTorr oxygen, yellow band in Figure 3A). In humid conditions, however, LaO-LFO is much more reactive toward water, with notable hydroxyl content at low RH. This is consistent with DFT calculations that report greater stability of hydroxylated LaO- versus FeO_2-LFO.[12] The amount of hydroxyls on the LaO surface remains roughly constant upon further increase of RH during the isobar, suggesting sites with a high binding strength for hydroxyls saturate at low RH.

The FeO_2-terminated surface has notably less hydroxyl species at low RH, which remains constant until ~10^{-3}% RH. At this point, H_2O_{ads} begins to form on the surface, and the amount of OH on FeO_2-LFO increases in parallel. This is in direct contrast to the hydroxyl behavior of LaO-LFO, but similar to that observed on Fe_3O_4 [39] and Fe_2O_3 [40] surfaces, where it was attributed to adsorbate-adsorbate interactions. In contrast, LaO-LFO adsorbs more water at a given RH with a lower onset RH; however, this does not significantly impact the formation of OH species.

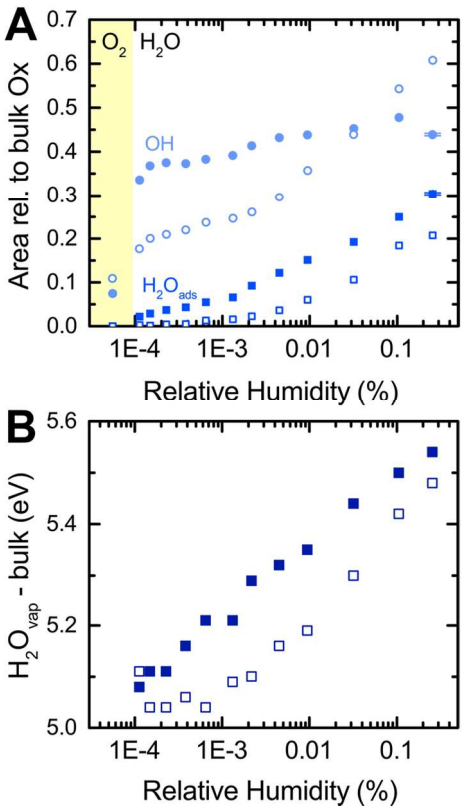

Figure 3. (A) Area of the OH (light blue, circles) and H_2O_{ads} (medium blue, squares) normalized to that of the bulk oxide as a function of RH probed by changing temperature in a 100 mTorr H_2O isobar. Dry conditions (300 °C in 100 mTorr O_2) are indicated with a yellow bar. LaO-LFO (solid) is more reactive toward water compared to FeO_2-LFO (open). (B) Location of the gas-phase H_2O_{vap} peak relative to the bulk oxygen peak for LaO-LFO (solid) and FeO_2-LFO (open) as a function of RH. The increase in binding energy corresponds to a decrease in sample work function, or formation of a surface dipole aiding photoelectron removal.

The use of AP-XPS also enables assessment of changes in the work function or surface dipole through shifts in the gas phase peak.[28,41] The H_2O_{gas} peak shifts to higher binding energy with RH, indicating a decrease in sample work function and/or formation of a surface dipole (Figure

3B). For example, adsorption of polar OH^- species have been shown to increase the surface potential of ceria.[41] This ~0.5 eV shift is similar to that observed on Fe_3O_4,[39] where DFT indicated adsorption of OH, H_2O, or co-adsorption of the two would lower the surface work function. For LFO, we highlight that the LaO-terminated surface exhibits a steady increase in gas phase binding energy with RH, while that of the FeO_2-terminated surface remains constant until ~10^{-3}% RH. This suggests that the decrease in work function is most influenced by the adsorption of polar water molecules, confirmed by its reversal upon decreasing the water pressure and desorbing H_2O_{ads} (Figure S10).

Further insight regarding changes in the electronic structure upon OH and H_2O adsorption can be obtained from the metal core levels and valence band. Aside from changes to the lanthanum-oxygen ionicity reflected in the satellite intensity (Figure S11),[42] the line shape of the La 4d and Fe 3p are negligibly affected by the formation of OH and H_2O_{ads} groups. However, their absolute binding energies (Figure 4) are affected, with shifts to a higher binding energy reflecting downward band bending. This shift is greatest for LaO-LFO, which also exhibits greater reactivity toward water. The change in spectral intensity at ~2.5 eV in FeO_2-LFO is not fully understood and merits further study.

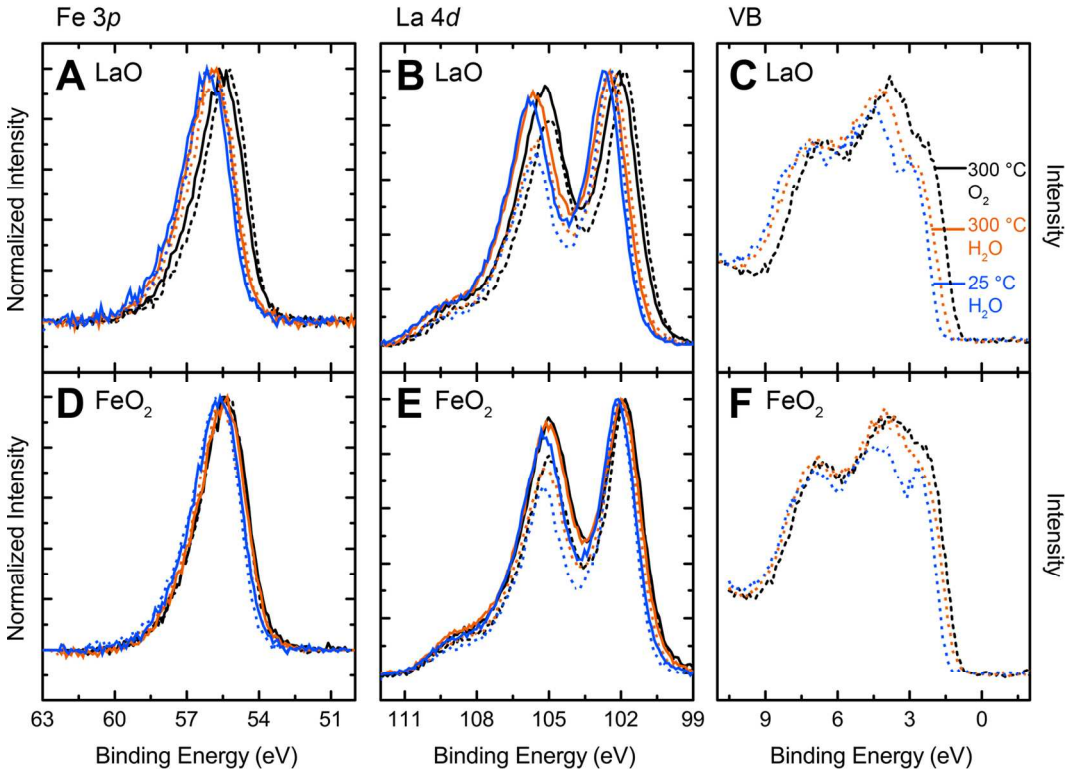

Figure 4. Noted Fe 3p, La 4d core levels and valence band (VB) for (A-C) LaO-LFO and (D-F) FeO_2-LFO. Solid lines are for 690 eV incident photon energy with a larger information depth than dashed lines for 350 eV. Conditions are 300 °C in 100 mTorr O_2 (black), 300 °C in 100 mTorr H_2O (orange) and 25 °C in 100 mTorr H_2O (blue). The shift to higher binding energies with increasing RH corresponds to downward band bending, and is greater for LaO-LFO.

In conclusion, we have presented a detailed study of the interaction between water and (001)-oriented $LaFeO_3$ films terminated with either the LaO or FeO_2 plane. Using ambient pressure X-ray photoelectron spectroscopy to probe the surface species present in equilibrium with gas phase water, we find greater hydroxylation of the LaO- versus FeO_2-LFO surface at low humidity, consistent with previous reports using DFT. However, the ultimately larger amount of OH on FeO_2-LFO at high humidity (commensurate with water adsorption) suggests adsorbate-

adsorbate interactions may play an important role in dictating reactivity. An additional surface oxygen species often observed on perovskites is present only on the LaO termination, such as a peroxo group that could protonate in humid conditions. Core level shifts and changes in the gas-phase water peak indicate a downward band bending/flattening and a decrease in work function, respectively, upon interaction with water. This experimental study of the impact of termination in complex oxides on chemical reactivity and the resultant electronic structure brings new insight to applications such as photoelectrocatalysis.

Experimental Methods

Film growth LFO/*n*-STO(001) heterojunctions were prepared using oxygen-assisted MBE. Films were grown at 600 ± 50°C at a rate of one monolayer (either LaO or FeO_2) every 43 seconds using effusion cells and alternately shuttering the La and Fe beams, with a mixed O/O_2 beam generated by an electron cyclotron resonance source continuously incident on the substrate.[43] A pair of 0.05% Nb-doped STO substrates (Crystec) were prepared side-by-side using a boiling deionized water treatment,[44] followed by an anneal in air at 1000 °C for 30 minutes. The samples were then cleaned in ozone on the bench and loaded into an oxide MBE system (DCA) with an appended x-ray photoelectron spectrometer (VG Scienta R3000 analyzer and monochromatic Al Kα x-ray source). The TiO_2 termination was confirmed using angle-resolved XPS measurements (Table S1). A single monolayer of SrO was then deposited using an effusion cell on one of the substrates to achieve the A-site termination, also confirmed by angle-resolved XPS.[19] Increments of three u.c. (1 u.c. = ~3.9Å) of LFO were then grown with a shuttering sequence configured to match the substrate termination (i.e. FeO_2 (LaO) layer deposited first on the SrO- (TiO_2-) terminated substrate) up to a total of 9 u.c.

Ambient pressure X-ray photoelectron Spectroscopy AP-XPS was collected at Beamline 9.3.2 at Lawrence Berkeley National Laboratory's (LBNL) Advanced Light Source (ALS).[45] LFO films were placed directly onto a ceramic heater and held in place by spring-loaded Inconel tips separated with an Al_2O_3 spacer. The film was grounded through a thermocouple pressed into a gold foil placed directly onto the sample surface for temperature measurements and isolated from the sample holder clip with an Al_2O_3 spacer. Further fitting details are provided in the Supplemental Information.

ASSOCIATED CONTENT

Supporting Information. Additional spectra, further spectral analysis, XPS fitting procedure, and TEM methods are available free of charge via the Internet at http://pubs.acs.org.

AUTHOR INFORMATION

Notes

The authors declare no competing financial interests.

ACKNOWLEDGMENT

APXPS measurements and analysis were supported for K.A.S. by the Linus Pauling Distinguished Post-doctoral Fellowship at Pacific Northwest National Laboratory (PNNL LDRD 69319), and for S.T. by the chemical imaging initiative, an LDRD program at PNNL. Film growth and characterization was supported at PNNL by the U.S. Department of Energy, Office of Science, Division of Materials Sciences and Engineering under Award No. 10122. The PNNL work was performed in the Environmental Molecular Sciences Laboratory (EMSL), a national science user facility sponsored by the Department of Energy's Office of Biological and

Environmental Research and located at Pacific Northwest National Laboratory. The ALS is supported by the Director, Office of Science, Office of Basic Energy Sciences of the US DOE at the Lawrence Berkeley National Laboratory under Contract DE-AC02-05CH11231.

REFERENCES

(1) Suntivich, J.; May, K. J.; Gasteiger, H. A.; Goodenough, J. B.; Shao-Horn, Y. A Perovskite Oxide Optimized for Oxygen Evolution Catalysis from Molecular Orbital Principles. *Science.* **2011**, *334*, 1383–1385.

(2) Suntivich, J.; Gasteiger, H. A.; Yabuuchi, N.; Nakanishi, H.; Goodenough, J. B.; Shao-Horn, Y. Design Principles for Oxygen-Reduction Activity on Perovskite Oxide Catalysts for Fuel Cells and Metal-Air Batteries. *Nat. Chem.* **2011**, *3*, 546–550.

(3) Man, I. C.; Su, H. Y.; Calle-Vallejo, F.; Hansen, H. A.; Martínez, J. I.; Inoglu, N. G.; Kitchin, J.; Jaramillo, T. F.; Nørskov, J. K.; Rossmeisl, J. Universality in Oxygen Evolution Electrocatalysis on Oxide Surfaces. *ChemCatChem* **2011**, *3*, 1159–1165.

(4) Jacobson, A. J. Materials for Solid Oxide Fuel Cells. *Chem. Mater.* **2010**, *22*, 660–674.

(5) May, K. J.; Fenning, D. P.; Ming, T.; Hong, W. T.; Lee, D.; Stoerzinger, K. A.; Biegalski, M. D.; Kolpak, A. M.; Shao-Horn, Y. Thickness-Dependent Photoelectrochemical Water Splitting on Ultrathin $LaFeO_3$ Films Grown on Nb:$SrTiO_3$. *J. Phys. Chem. Lett.* **2015**, *6*, 977–985.

(6) Peng, Q.; Wang, J.; Wen, Y. W.; Shan, B.; Chen, R. Surface Modification of $LaFeO_3$ by Co-Pi Electrochemical Deposition as an Efficient Photoanode under Visible Light. *RSC Adv.* **2016**, *6*, 26192–26198.

(7) Parida, K. M.; Reddy, K. H.; Martha, S.; Das, D. P.; Biswal, N. Fabrication of Nanocrystalline $LaFeO_3$: An Efficient Sol-Gel Auto-Combustion Assisted Visible Light Responsive Photocatalyst for Water Decomposition. *Int. J. Hydrogen Energy* **2010**, *35*, 12161–12168.

(8) Fergus, J. W. Perovskite Oxides for Semiconductor-Based Gas Sensors. *Sensors Actuators, B Chem.* **2007**, *123*, 1169–1179.

(9) Toan, N. N.; Saukko, S.; Lantto, V. Gas Sensing with Semiconducting Perovskite Oxide $LaFeO_3$. *Phys. B Condens. Matter* **2003**, *327*, 279–282.

(10) Zhao, J.; Liu, Y.; Li, X.; Lu, G.; You, L.; Liang, X.; Liu, F.; Zhang, T.; Du, Y. Highly Sensitive Humidity Sensor Based on High Surface Area Mesoporous $LaFeO_3$ Prepared by a Nanocasting Route. *Sensors Actuators, B Chem.* **2013**, *181*, 802–809.

(11) Nenning, A.; Navickas, E.; Hutter, H.; Fleig, J. Water-Induced Decoupling of Tracer and Electrochemical Oxygen Exchange Kinetics on Mixed Conducting Electrodes. *J. Phys. Chem. Lett.* **2016**, *7*, 2826–2831.

(12) Stoerzinger, K. A.; Hong, W. T.; Azimi, G.; Giordano, L.; Lee, Y. L.; Crumlin, E. J.; Biegalski, M. D.; Bluhm, H.; Varanasi, K. K.; Shao-Horn, Y. Reactivity of Perovskites with Water: Role of Hydroxylation in Wetting and Implications for Oxygen Electrocatalysis. *J. Phys. Chem. C* **2015**, *119*, 18504–18512.

(13) Rubasinghege, G.; Elzey, S.; Baltrusaitis, J.; Jayaweera, P. M.; Grassian, V. H. Reactions on Atmospheric Dust Particles: Surface Photochemistry and Size-Dependent Nanoscale Redox Chemistry. *J. Phys. Chem. Lett.* **2010**, *1*, 1729–1737.

(14) Henderson, M. A. The Interaction of Water With Solid Surfaces : Fundamental Aspects. *Surf. Sci. Rep.* **2002**, *46*, 1–308.

(15) Brown Jr., G. E.; Henrich, V. E.; Casey, W. H.; Clark, D. L.; Eggleston, C.; Felmy, A.; Goodman, D. W.; Graetzel, M.; Maciel, G.; McCarthy, M. I.; et al. Metal Oxide Surfaces and Their Interactions with Aqueous Solutions and Microbial Organisms. *Chem. Rev.* **1999**, *99*, 77–174.

(16) Von Rudorff, G. F.; Jakobsen, R.; Rosso, K. M.; Blumberger, J. Fast Interconversion of Hydrogen Bonding at the Hematite (001)-Liquid Water Interface. *J. Phys. Chem. Lett.* **2016**, *7*, 1155–1160.

(17) Stoerzinger, K. A.; Hong, W. T.; Crumlin, E. J.; Bluhm, H.; Biegalski, M. D.; Shao-Horn, Y. Water Reactivity on the $LaCoO_3$ (001) Surface: An Ambient Pressure X-Ray Photoelectron Spectroscopy Study. *J. Phys. Chem. C* **2014**, *118*, 19733–19741.

(18) Stoerzinger, K. A.; Hong, W. T.; Crumlin, E. J.; Bluhm, H.; Shao-Horn, Y. Insights into Electrochemical Reactions from Ambient Pressure Photoelectron Spectroscopy. *Acc. Chem. Res.* **2015**, *48*, 2976–2983.

(19) Comes, R.; Chambers, S. Interface Structure, Band Alignment, and Built-In Potentials at $LaFeO_3$/n-$SrTiO_3$ Heterojunctions. *Phys. Rev. Lett.* **2016**, *117*, 226802.

(20) Nakamura, K.; Mashiko, H.; Yoshimatsu, K.; Ohtomo, A. Impact of Built-in Potential across LaFeO3/SrTiO3 Heterojunctions on Photocatalytic Activity. *Appl. Phys. Lett.* **2016**, *108*, 211605.

(21) Nakamura, M.; Kagawa, F.; Tanigaki, T.; Park, H. S.; Matsuda, T.; Shindo, D.; Tokura,

Y.; Kawasaki, M. Spontaneous Polarization and Bulk Photovoltaic Effect Driven by Polar Discontinuity in LaFeO3/SrTiO3 Heterojunctions. *Phys. Rev. Lett.* **2016**, *116*, 156801.

(22) Xu, P.; Han, W.; Rice, P. M.; Jeong, J.; Samant, M. G.; Mohseni, K.; Meyerheim, H. L.; Ostanin, S.; Maznichenko, I. V; Mertig, I.; et al. Reversible Formation of 2D Electron Gas at the $LaFeO_3/SrTiO_3$ Interface via Control of Oxygen Vacancies. *Adv. Mater.* **2017**, 1604447.

(23) Jacobs, R.; Booske, J.; Morgan, D. Understanding and Controlling the Work Function of Perovskite Oxides Using Density Functional Theory. *Adv. Funct. Mater.* **2016**, *26*, 5471–5482.

(24) Makowski, M. J.; Galhenage, R. P.; Langford, J.; Hemminger, J. C. Liquid-Jet X-Ray Photoelectron Spectra of TiO2 Nanoparticles in an Aqueous Electrolyte Solution. *J. Phys. Chem. Lett.* **2016**, *7*, 1732–1735.

(25) Starr, D. E.; Liu, Z.; Hävecker, M.; Knop-Gericke, A.; Bluhm, H. Investigation of Solid/vapor Interfaces Using Ambient Pressure X-Ray Photoelectron Spectroscopy. *Chem. Soc. Rev.* **2013**, *42*, 5833–5857.

(26) Crumlin, E. J.; Bluhm, H.; Liu, Z. In Situ Investigation of Electrochemical Devices Using Ambient Pressure Photoelectron Spectroscopy. *J. Electron Spectros. Relat. Phenomena* **2013**, *190*, 84–92.

(27) Lichterman, M. F.; Hu, S.; Richter, M. H.; Crumlin, E.; Axnanda, S.; Favaro, M.; Drisdell, W. S.; Hussain, Z.; Mayer, T.; Brunschwig, B. S.; et al. Direct Observation of the Energetics at a Semiconductor/Liquid Junction by Operando X-Ray Photoelectron

Spectroscopy. *Energy Environ. Sci.* **2015**, *8*, 2409–2416.

(28) Axnanda, S.; Scheele, M.; Crumlin, E.; Mao, B. H.; Chang, R.; Rani, S.; Faiz, M.; Wang, S. D.; Alivisatos, A. P.; Liu, Z. Direct Work Function Measurement by Gas Phase Photoelectron Spectroscopy and Its Application on PbS Nanoparticles. *Nano Lett.* **2013**, *13*, 6176–6182.

(29) Gonzalez-Elipe, A. R.; Espinos, J. P.; Fernandez, A.; Munuera, G. XPS Study of the Surface Carbonation/hydroxylation State of Metal Oxides. *Appl. Surf. Sci.* **1990**, *45*, 103–108.

(30) Merino, N. A.; Barbero, B. P.; Eloy, P.; Cadús, L. E. $La_{1-x}Ca_xCoO_3$ Perovskite-Type Oxides: Identification of the Surface Oxygen Species by XPS. *Appl. Surf. Sci.* **2006**, *253*, 1489–1493.

(31) Flynn, B. T.; Zhang, K. H. L.; Shutthanandan, V.; Varga, T.; Colby, R. J.; Oleksak, R. P.; Manandhar, S.; Engelhard, M. H.; Chambers, S. A.; Henderson, M. A.; et al. Growth and Surface Modification of $LaFeO_3$ Thin Films Induced by Reductive Annealing. *Appl. Surf. Sci.* **2015**, *330*, 309–315.

(32) Becerra-Toledo, A. E.; Enterkin, J. A.; Kienzle, D. M.; Marks, L. D. Water Adsorption on SrTiO3(001): II. Water, Water, Everywhere. *Surf. Sci.* **2012**, *606*, 791–802.

(33) Mefford, J. T.; Hardin, W. G.; Dai, S.; Johnston, K. P.; Stevenson, K. J. Anion Charge Storage through Oxygen Intercalation in $LaMnO_3$ Perovskite Pseudocapacitor Electrodes. *Nat. Mater.* **2014**, *13*, 726–732.

(34) Geneste, G.; Morillo, J.; Finocchi, F. Adsorption and Diffusion of Mg, O, and O_2 on the

MgO(001) Flat Surface. *J. Chem. Phys.* **2005**, *122*, 174707.

(35) Worayingyong, A.; Kangvansura, P.; Ausadasuk, S.; Praserthdam, P. The Effect of Preparation: Pechini and Schiff Base Methods, on Adsorbed Oxygen of $LaCoO_3$ Perovskite Oxidation Catalysts. *Colloids Surfaces A Physicochem. Eng. Asp.* **2008**, *315*, 217–225.

(36) Kaliaguine, S.; Van Neste, A.; Szabo, V.; Gallot, J. E.; Bassir, M.; Muzychuk, R. Perovskite-Type Oxides Synthesized by Reactive Grinding. Part I. Preparation and Characterization. *Appl. Catal. A Gen.* **2001**, *209*, 345–358.

(37) Newberg, J. T.; Starr, D. E.; Yamamoto, S.; Kaya, S.; Kendelewicz, T.; Mysak, E. R.; Porsgaard, S.; Salmeron, M. B.; Brown, G. E.; Nilsson, A.; et al. Formation of Hydroxyl and Water Layers on MgO Films Studied with Ambient Pressure XPS. *Surf. Sci.* **2011**, *605*, 89–94.

(38) Corberán, V. C.; Tejuca, L. G.; Bell, A. T. Surface Reactivity of Reduced $LaFeO_3$ as Studied by TPD and IR Spectroscopies of CO, CO_2 and H_2. *J. Mater. Sci.* **1989**, *24*, 4437–4442.

(39) Kendelewicz, T.; Kaya, S.; Newberg, J. T.; Bluhm, H.; Mulakaluri, N.; Moritz, W.; Scheffler, M.; Nilsson, A.; Pentcheva, R.; Brown, G. E. X-Ray Photoemission and Density Functional Theory Study of the Interaction of Water Vapor with the Fe_3O_4 (001) Surface at Near-Ambient Conditions. *J. Phys. Chem. C* **2013**, *117*, 2719–2733.

(40) Yamamoto, S.; Kendelewicz, O. T.; Newberg, J. T.; Ketteler, G.; Starr, D. E.; Mysak, E. R.; Andersson, K. J.; Ogasawara, H.; Bluhm, H.; Salmeron, M.; et al. Water Adsorption

on α-Fe_2O_3 (0001) at near Ambient Conditions. *J. Phys. Chem. C* **2010**, *114*, 2256–2266.

(41) Feng, Z. A.; Balaji Gopal, C.; Ye, X.; Guan, Z.; Jeong, B.; Crumlin, E.; Chueh, W. C. Origin of Overpotential-Dependent Surface Dipole at CeO_{2-x}/Gas Interface During Electrochemical Oxygen Insertion Reactions. *Chem. Mater.* **2016**, *28*, 6233–6242.

(42) Sunding, M. F.; Hadidi, K.; Diplas, S.; Løvvik, O. M.; Norby, T. E.; Gunnæs, A. E. XPS Characterisation of in Situ Treated Lanthanum Oxide and Hydroxide Using Tailored Charge Referencing and Peak Fitting Procedures. *J. Electron Spectros. Relat. Phenomena* **2011**, *184*, 399–409.

(43) Comes, R. B.; Xu, P.; Jalan, B.; Chambers, S. A. Band Alignment of Epitaxial $SrTiO_3$ Thin Films with $(LaAlO_3)_{0.3}$-$(Sr_2AlTaO_6)_{0.7}$ (001). *Appl. Phys. Lett.* **2015**, *107*, 131601.

(44) Chambers, S. A.; Droubay, T. C.; Capan, C.; Sun, G. Y. Unintentional F Doping of $SrTiO_3$(001) Etched in HF Acid-Structure and Electronic Properties. *Surf. Sci.* **2012**, *606*, 554–558.

(45) Grass, M. E.; Karlsson, P. G.; Aksoy, F.; Lundqvist, M.; Wannberg, B.; Mun, B. S.; Hussain, Z.; Liu, Z. New Ambient Pressure Photoemission Endstation at Advanced Light Source Beamline 9.3.2. *Rev. Sci. Instrum.* **2010**, *81*, 53106.

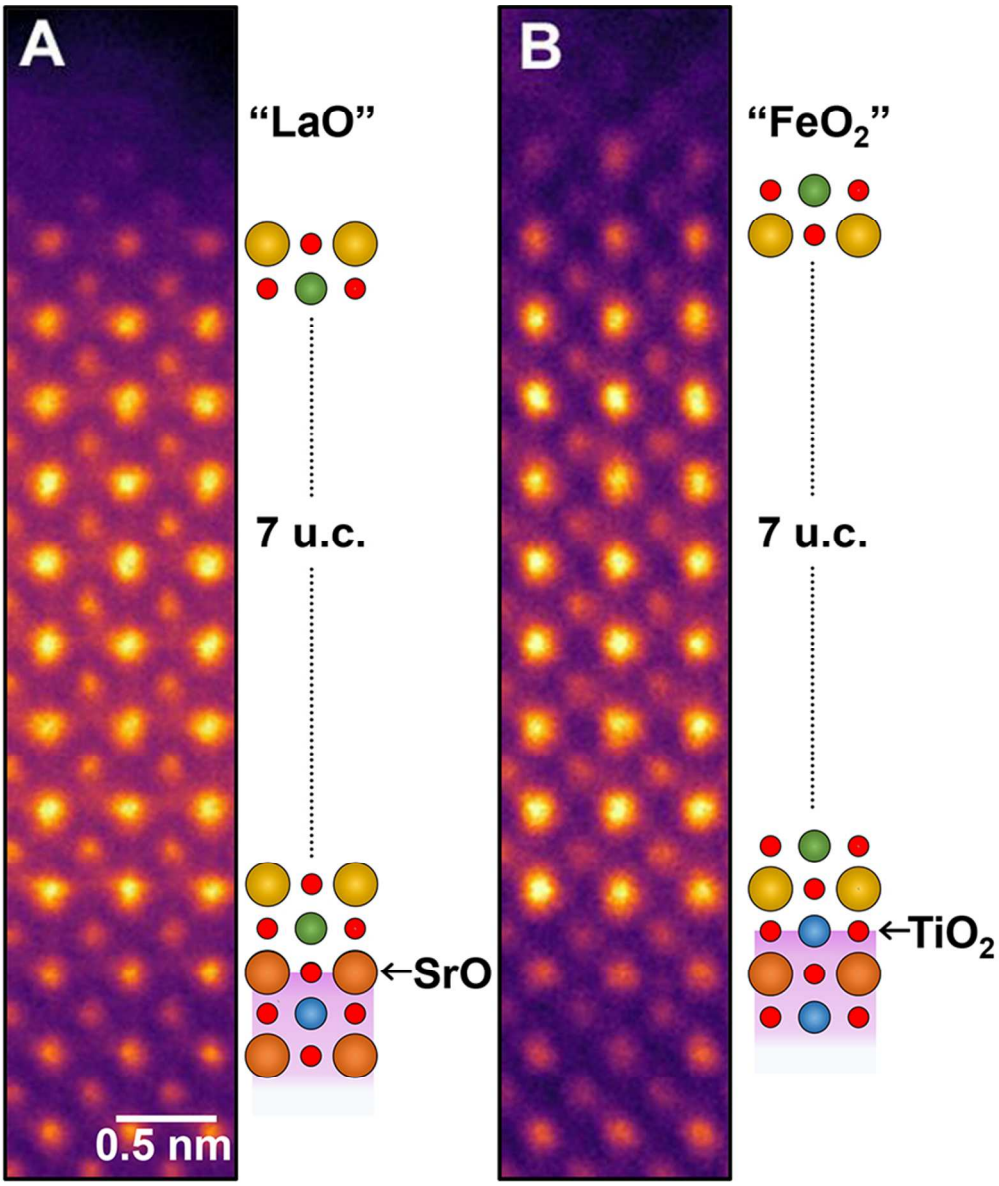

Figure 1. Colorized cross-sectional STEM-HAADF images and schematics of the 9 unit cell (u.c.) $LaFeO_3$/Nb:$SrTiO_3$ films fabricated by oxygen assisted MBE. LaO-LFO was grown on a SrO-terminated substrate (A), and FeO_2-LFO was grown on a TiO_2-terminated one (B). Surface terminations were confirmed by angle resolved XPS (Table S1).[19]

Figure 1
76x89mm (300 x 300 DPI)

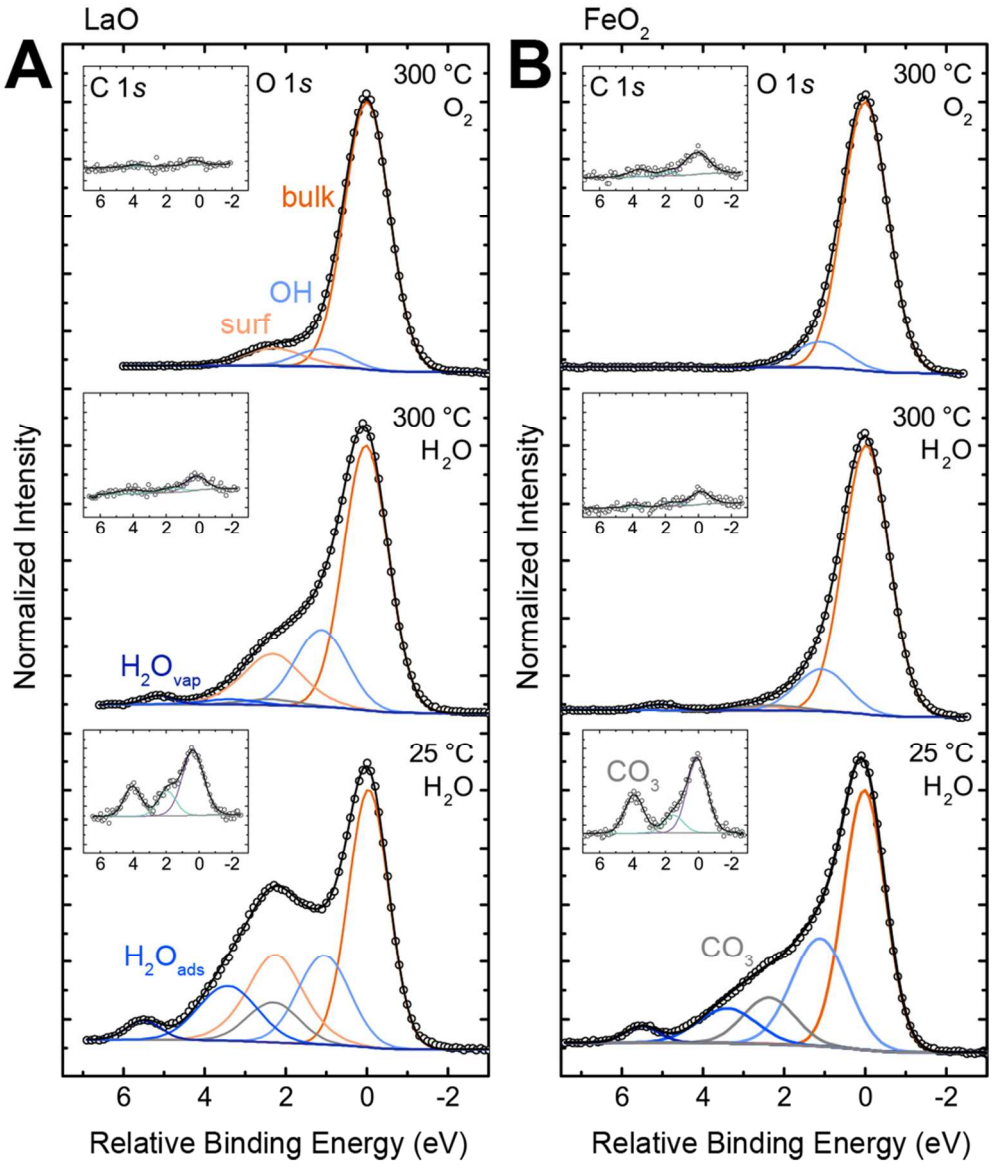

Figure 2. O 1s spectra and C 1s spectra (inset) for (A) LaO-LFO and (B) FeO_2-LFO at 300 °C in 100 mTorr O_2 (top), 300 °C in 100 mTorr H_2O (middle) and 25 °C in 100 mTorr H_2O (bottom). Raw data are shown as points with fitted components and envelope (black) as lines. O 1s components correspond to the bulk oxide (orange), hydroxide (light blue), carbonate (gray), surface (peach), adsorbed water (medium blue), and gas phase water (dark blue). C 1s components correspond to carbonate (gray), adventitious carbon (purple), and an intermediate carbon oxidation (teal). The binding energy scale is shown relative to the bulk oxide (O 1s) and adventitious carbon (C 1s) to better illustrate relative offsets of species in fitting.

Figure 2
107x125mm (300 x 300 DPI)

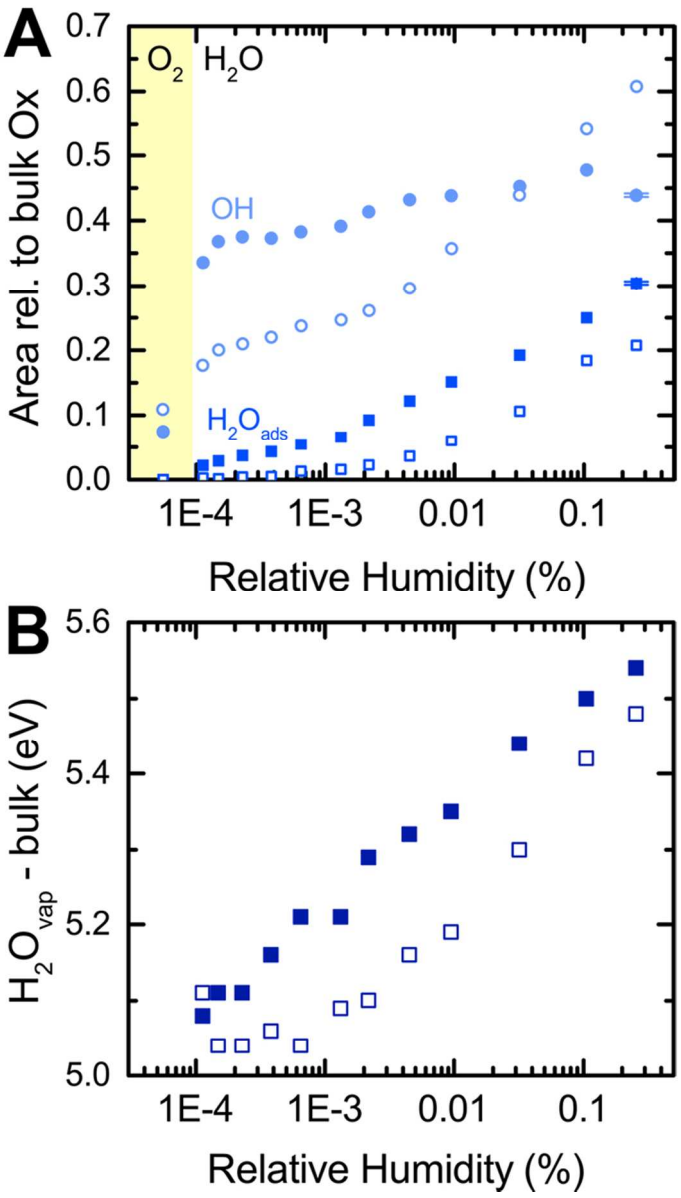

Figure 3. (A) Area of the OH (light blue, circles) and H_2O_{ads} (medium blue, squares) normalized to that of the bulk oxide as a function of RH probed by changing temperature in a 100 mTorr H_2O isobar. Dry conditions (300 °C in 100 mTorr O_2) are indicated with a yellow bar. LaO-LFO (solid) is more reactive toward water compared to FeO_2-LFO (open). (B) Location of the gas-phase H_2O_{vap} peak relative to the bulk oxygen peak for LaO-LFO (solid) and FeO_2-LFO (open) as a function of RH. The increase in binding energy corresponds to a decrease in sample work function, or formation of a surface dipole aiding photoelectron removal.
Figure 3
60x107mm (300 x 300 DPI)

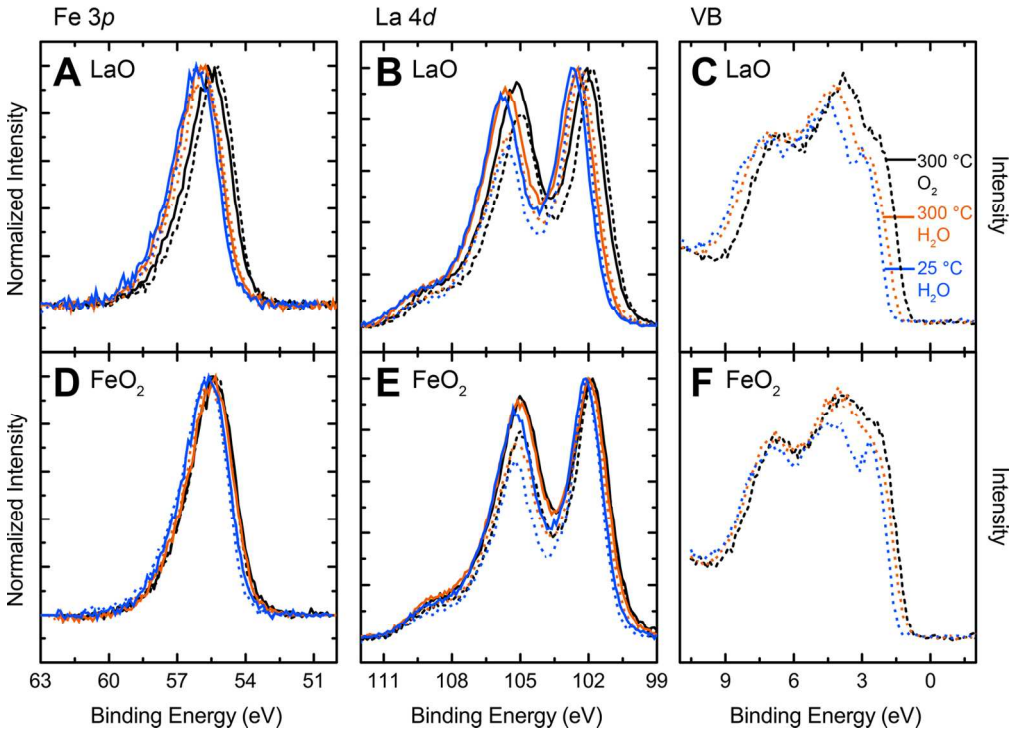

Figure 4. Noted Fe 3p, La 4d core levels and valence band (VB) for (A-C) LaO-LFO and (D-F) FeO_2-LFO. Solid lines are for 690 eV incident photon energy with a larger information depth than dashed lines for 350 eV. Conditions are 300 °C in 100 mTorr O_2 (black), 300 °C in 100 mTorr H_2O (orange) and 25 °C in 100 mTorr H_2O (blue). The shift to higher binding energies with increasing RH corresponds to downward band bending, and is greater for LaO-LFO.

Figure 4.
139x102mm (300 x 300 DPI)